Bound states in the continuum and polarization singularities in periodic arrays of dielectric rods

Evgeny N. Bulgakov and Dmitrii N. Maksimov
Reshetnev Siberian State University of Science and Technology, 660037, Krasnoyarsk, Russia
and Kirensky Institute of Physics, Federal Research Center KSC SB RAS, 660036, Krasnoyarsk, Russia
(Received 15 November 2017; published 22 December 2017)

We consider optical bound states in the continuum (BICs) in periodic arrays of dielectric rods. The full classification of BICs in the above system is provided, including the modes propagating along the axes of the rods and bidirectional BICs propagating both along the axes of the rods and the axis of periodicity. It is shown that the leaky zones supporting the BICs generally have elliptically polarized far-field radiation patterns, with the polarization ellipses collapsing on approach to the BICs in momentum space. That allowed us to apply the concept of polarization singularities and demonstrate that the BICs possess a topological charge defined as the winding number of the polarization direction [Phys. Rev. Lett. **113**, 257401 (2014)]. It is found that the evolution of the BICs, including their creation and annihilation, under variation of geometric parameters is controlled by the topological charge. Three scenarios of such evolution for different leaky zones are described. Finally, it is shown that the topological properties of the BICs can be extracted from transmission spectra when the system is illuminated by a plane wave of circular polarization.

DOI: 10.1103/PhysRevA.96.063833

I. INTRODUCTION

The spectrum of an optical system coupled to radiation channels is generally described by leaky zones, i.e., dispersion branches of the complex resonant eigenfrequencies of Maxwell's operator with radiation boundary conditions in the far zone. With a certain set of parameters the leaky zones may host exceptional points in which the imaginary part of the resonant eigenfrequency equals zero and the resonant state is a localized solution decoupled from the outgoing waves in the ambient medium. Such localized solutions are known as bound states in the continuum (BICs) [1]. Recently, the immense progress in handling photonic crystals encouraged extensive studies on BICs in various periodic structures, both experimental [2–8] and theoretical [9–20]. These studies are predominantly motivated by potential applications to resonant enhancement [21–24], lasing [25,26], and filtering of light [27,28].

One remarkable property of BICs is their robustness against small perturbations, given that the symmetry of the supporting structure is preserved [29–31]. This robustness indicates the presence of a topological charge that stabilizes the BICs against perturbations [29,30]. In 2014 Bo Zhen *et al.* [29] demonstrated that BICs in dielectric slabs are vortex centers of the polarization directions of far-field radiation in momentum space. The vortices in two-dimensional vector fields are characterized by topological charge, quantized winding angle of the field around the vortex core [32]. Since the topological charge must be preserved, the evolution, creation, and annihilation of BICs is controlled by topological charge prescribed to the leaky zones supporting the BICs. The topological properties of BICs have recently attracted a great deal of attention [8,30,33–35]. In particular, topologically protected polarization conversion was theoretically predicted in Ref. [35], while the vortices in momentum space were experimentally observed in Ref. [34].

In this paper we revisit the spectral properties of periodic arrays of dielectric rods to address the polarization singularities of the leaky zones supporting optical BICs. The BICs in arrays of dielectric rods of circular cross section were first theoretically predicted in Ref. [36]. Later on, an extensive numerical study of BICs in the above system was undertaken with the BIC existence domains identified [37]. Besides its simplicity, one of the advantages of the system under scrutiny is the opportunity to solve the scattering problem with the cylindrical harmonics expansion method [38,39] which provides a numerically efficient approach to finding reflection and transmission spectra and electromagnetic (EM) field patterns for full wave three-dimensional (3D) scattering problem.

The article is organized as follows: In Sec. II we describe the setup, review the scattering theory for periodic arrays of dielectric rods, and describe a numerical method for finding transmission or reflection spectrum to be used for computing the BICs. In Sec. III we collect our numerical results on BICs in arrays of dielectric rods. In Sec. IV we consider the polarization properties of the leaky bands, demonstrating that the far-field radiation is in general elliptically polarized with the polarization ellipses collapsing in the vicinity of the BICs. Then, following Ref. [29], the BICs are described as polarization singularities, i.e., vortices in momentum space. The topological classification of the BICs is also provided. In Sec. V we consider the evolution of BICs under variation of geometric parameters of the system to show that creation or annihilation of BICs obeys the rule of the topological charge conservation. In Sec. VI we demonstrate that the topological charge can be detected in the far-field measurements if the system is illuminated by a plane waves whose wave vector bypasses the point of the polarization singularity along a certain closed contour in momentum space. The summary of our findings is provided in Sec. VII.

II. INTERACTION MATRIX OF SCATTERING SYSTEM

We consider an array of dielectric cylinders of radius R and permittivity ϵ in air. The cylinders are infinitely long in the z direction, parallel to each other, and periodically spaced with distance a along the x axis on $x0y$ plane as shown in

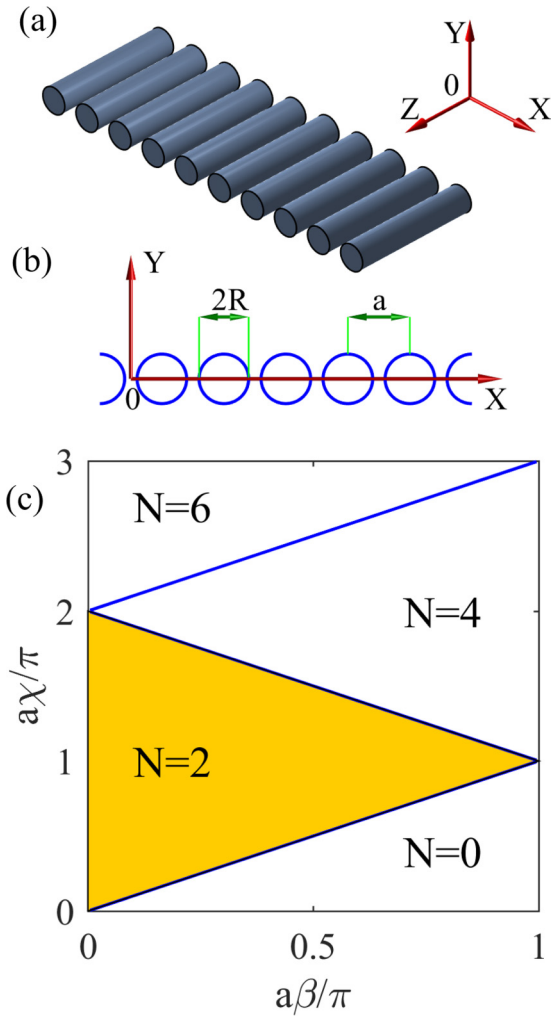

FIG. 1. Periodic array of dielectric cylinders. (a) Three-dimensional plot of the array. (b) The array in $x0y$ plane. (c) Number of scattering channels in the space of Bloch vector β and χ. The yellow shaded area is the sector of the parametric space where only two scattering channels are open.

Figs. 1(a) and 1(b). The far-field $y \to \pm\infty$ scattering channels are transverse magnetic (TM) waves with the magnetic vector orthogonal to the z axis, and transverse electric (TE) waves with electric vector orthogonal to the z axis. The far-field TM scattering channels can be written as

$$\begin{aligned}\mathbf{E}_{TM} &= \frac{1}{k_0}\left(\frac{-k_z\beta}{\chi}, \frac{-k_z k_y}{\chi}, \chi\right) e^{i(\beta x + k_y|y| + k_z z)},\\ \mathbf{H}_{TM} &= \frac{1}{k_0}\left(\frac{-k_0 k_y}{\chi}, \frac{k_0\beta}{\chi}, 0\right) e^{i(\beta x + k_y|y| + k_z z)},\end{aligned} \tag{1}$$

while for TE modes we have

$$\begin{aligned}\mathbf{E}_{TE} &= \frac{1}{k_0}\left(\frac{k_0 k_y}{\chi}, \frac{-k_0\beta}{\chi}, 0\right) e^{i(\beta x + k_y|y| + k_z z)},\\ \mathbf{H}_{TE} &= \frac{1}{k_0}\left(\frac{-k_z\beta}{\chi}, \frac{-k_z k_y}{\chi}, \chi\right) e^{i(\beta x + k_y|y| + k_z z)},\end{aligned} \tag{2}$$

where k_0 is the vacuum wave number (frequency), k_y,k_z are the components of the wave vector along the y,z axes, β is the Bloch wave number along the x axis, and

$$\chi^2 = k_0^2 - k_z^2. \tag{3}$$

Notice that

$$\begin{aligned}\mathbf{E}_{TE}^\dagger \mathbf{E}_{TM} &= \mathbf{H}_{TE}^\dagger \mathbf{H}_{TM} = 0,\\ \mathbf{E}_{TM}^\dagger \mathbf{E}_{TM} &= \mathbf{H}_{TM}^\dagger \mathbf{H}_{TM} = 1,\\ \mathbf{E}_{TE}^\dagger \mathbf{E}_{TE} &= \mathbf{H}_{TE}^\dagger \mathbf{H}_{TE} = 1.\end{aligned} \tag{4}$$

Due to the periodicity, the spectrum of the scattering channels obeys the following dispersion relationship:

$$k_0^2 = k_z^2 + k_y^2 + (\beta + 2\pi l)^2, \quad l = 0, \pm 1, \pm 2, \ldots. \tag{5}$$

Throughout the paper we will stay in the range

$$a\beta < a\chi < 2\pi - a\beta,$$

where only two (one TE and one TM) scattering channels are open, as shown in Fig. 1(c).

Let us now review the scattering theory for linear arrays of dielectric rods. We will follow the approach by Ref. [38]. The key idea of the approach is to expresses the scattering matrix of an infinite periodic array through that of a single rod. The scattering solution for a single rod is well known in the literature with the key figure of merit being matrix $\widehat{T}(m)$ that links the amplitudes of the impinging TM or TE waves e_m or h_m to the amplitudes of the outgoing TM or TE waves a_m or b_m with orbital angular momentum m:

$$\begin{bmatrix} a_m \\ b_m \end{bmatrix} = \widehat{T}(m) \begin{bmatrix} e_m \\ h_m \end{bmatrix}. \tag{6}$$

The EM field outside the rods is given by

$$E_z = e^{ik_z z} \sum_{m=-\infty}^{\infty} \left[a_m H_m^{(1)}(\chi r) + e_m J_m(\chi r)\right] e^{\mathrm{i}m\varphi} \tag{7}$$

for TM-waves, and

$$H_z = e^{ik_z z} \sum_{m=-\infty}^{\infty} \left[b_m H_m^{(1)}(\chi r) + h_m J_m(\chi r)\right] e^{\mathrm{i}m\varphi} \tag{8}$$

for TE-waves, where $J_m(\chi r)$ and $H_m^{(1)}(\chi r)$ are Bessel and Hankel functions, respectively. Now assume that the rod is illuminated from the far zone by TM or TE plane waves (12) with wave vector $\mathbf{k} = (\beta, k_y, k_z)$. To match the incident and the outgoing fields, the incident wave should be expanded over the Bessel functions. For the TM waves we have

$$e_m = e_{(\mathrm{in})}(-i)^m e^{-\mathrm{i}m\varphi_{\mathrm{in}}}, \quad h_m = 0, \tag{9}$$

while for TE waves the expansion coefficients are the following:

$$e_m = 0, \quad h_m = h_{(\mathrm{in})}(-i)^m e^{-\mathrm{i}m\varphi_{\mathrm{in}}}, \tag{10}$$

with φ_{in} being the azimuthal angle of incidence in the $x0y$ plane,

$$\tan\varphi_{\mathrm{in}} = (k_y/\beta),$$

and $e_{(\mathrm{in})}$, $h_m = h_{(\mathrm{in})}$ as the amplitudes of the incident TM or TE waves.

For scattering by a single rod matrix $\hat{T}_m$ can be written as

$$\widehat{T}(m) = \begin{bmatrix} \tau_{e,e}(m), & \tau_{e,h}(m) \\ \tau_{h,e}(m), & \tau_{h,h}(m) \end{bmatrix}. \tag{11}$$

The coefficients are obtained in the closed form as

$$\begin{aligned}
\tau_{e,e}(m) &= -\frac{J_m(w)}{H_m^{(1)}(w)} \frac{\Delta_m^{(2)}\Delta_m^{(3)} - K_m^2}{\Delta_m^{(1)}\Delta_m^{(2)} - K_m^2}, \\
\tau_{e,h}(m) &= -\tau_{h,e}(m) = \frac{2k_0}{\pi w^2 k} \frac{K_m}{\left[H_m^{(1)}(w)\right]^2} \frac{1}{\Delta_m^{(1)}\Delta_m^{(2)} - K_m^2}, \\
\tau_{h,h}(m) &= -\frac{J_m(w)}{H_m^{(1)}(w)} \frac{\Delta_m^{(4)}\Delta_m^{(1)} - K_m^2}{\Delta_m^{(1)}\Delta_m^{(2)} - K_m^2},
\end{aligned} \tag{12}$$

with

$$\begin{aligned}
\Delta_m^{(1)} &= \frac{J_m'(u)}{uJ_m(u)} - \frac{1}{\epsilon}\frac{H_m'^{(1)}(w)}{wH_m^{(1)}(w)}, \\
\Delta_m^{(2)} &= \frac{J_m'(u)}{uJ_m(u)} - \frac{H_m'^{(1)}(w)}{wH_m^{(1)}(w)}, \\
\Delta_m^{(3)} &= \frac{J_m'(u)}{uJ_m(u)} - \frac{1}{\epsilon}\frac{J_m'(w)}{wJ_m(w)}, \\
\Delta_m^{(4)} &= \frac{J_m'(u)}{uJ_m(u)} - \frac{J_m'(w)}{wJ_m(w)}, \\
K_m &= \frac{mk_z}{\sqrt{\epsilon}k_0}\left(\frac{1}{u^2} - \frac{1}{w^2}\right), \\
w &= R\chi, \quad u = R\sqrt{\epsilon k_0^2 - k_z^2}.
\end{aligned} \tag{13}$$

In the case of a periodic array the scattering problem can be reduced to the scattering by a single cylinder [38] through a modified set of equations

$$\begin{cases} (\widehat{\mathbb{1}} - \widehat{\tau}_{e,e}\widehat{L}^{(x)})\mathbf{a} - \widehat{\tau}_{e,h}\widehat{L}^{(x)}\mathbf{b} = \widehat{\tau}_{e,e}\mathbf{e} + \widehat{\tau}_{e,h}\mathbf{h} \\ \widehat{\tau}_{e,h}\widehat{L}^{(x)}\mathbf{a} + (\widehat{\mathbb{1}} - \widehat{\tau}_{h,h}\widehat{L}^{(x)})\mathbf{b} = -\widehat{\tau}_{e,h}\mathbf{e} + \widehat{\tau}_{h,h}\mathbf{h}, \end{cases} \tag{14}$$

where $\mathbf{a}$, $\mathbf{b}$, $\mathbf{e}$, and $\mathbf{h}$ are the vectors of coefficients a_m, b_m, e_m, and h_m; $\widehat{\tau}_{p,p'}$, $p = e,h$ are diagonal matrices $\widehat{\tau}_{p,p'} = \mathrm{diag}(\tau_{p,p'})$; and $\widehat{L}^{(x)}$ is the matrix which accounts for multiple scattering events between the rods in the form of an infinite lattice sum along the x axis,

$$L_{m',m}^{(x)} = \sum_{l=0}^{\infty} H_{m'-m}^{(1)}(\chi R)[e^{il\beta R} + (-1)^{m'-m}e^{-il\beta R}]. \tag{15}$$

Equation (14) can be rewritten in a compact form,

$$\widehat{L}\mathbf{c} = \mathbf{f}, \tag{16}$$

where $\mathbf{c} = [\mathbf{a},\mathbf{b}]$, $\mathbf{f} = [\mathbf{e},\mathbf{h}]$, and

$$\widehat{L} = \widehat{T}^{-1}\begin{Bmatrix} \widehat{\mathbb{1}} - \widehat{\tau}_{e,e}\widehat{L}^{(x)} & -\widehat{\tau}_{e,h}\widehat{L}^{(x)} \\ \widehat{\tau}_{e,h}\widehat{L}^{(x)} & \widehat{\mathbb{1}} - \widehat{\tau}_{h,h}\widehat{L}^{(x)} \end{Bmatrix}, \tag{17}$$

with

$$\widehat{T} = \begin{Bmatrix} \widehat{\tau}_{e,e} & \widehat{\tau}_{e,h} \\ -\widehat{\tau}_{e,h} & \widehat{\tau}_{h,h} \end{Bmatrix}. \tag{18}$$

In what follows $\widehat{L}$ is referred to as the interaction matrix of the scattering system.

TABLE I. BICs in arrays of dielectric rods at $\epsilon = 15$. The mode profiles of the BICs are shown in Fig. 2.

	R/a	ak_z	$a\beta$	ak_0	q
BIC 1	0.449	0	0	3.5183	−1
BIC 2	0.44411	0	0	2.8299	0
BIC 3	0.43	0	0	3.602	+1
BIC 4	0.47	0	0	3.4502	+1
BIC 5	0.45	0	0.48099	3.4718	+1
BIC 6	0.439	0	0.25858	2.8659	+1
BIC 7	0.3	0	1.0980	3.1952	−1
BIC 8	0.34	0	0.478	2.7802	+1
BIC 9	0.4505	0.56795	0	3.53	+1
BIC 10	0.439	1.2871	0	2.8852	−1
BIC 11	0.3	1.1904	0.96714	3.1966	+1

The solution of the scattering problem can found from Eq. (16). Finally, for reflection or transmission amplitudes of plane waves in the TM and TE scattering channels $e_{(r,t)}$, $h_{(r,t)}$ we have

$$\begin{aligned}
e_{(r)} &= \mathbf{u}_{(+)}^{\dagger}\mathbf{a}, \quad e_{(t)} = e_{(\mathrm{in})} + \mathbf{u}_{(-)}^{\dagger}\mathbf{a}, \\
h_{(r)} &= \mathbf{u}_{(+)}^{\dagger}\mathbf{b}, \quad h_{(t)} = h_{(\mathrm{in})} + \mathbf{u}_{(-)}^{\dagger}\mathbf{b},
\end{aligned} \tag{19}$$

where

$$\mathbf{u}_{(\pm)} = \left[\frac{2(-i)^{m-1}}{\chi a \sin(\varphi_{\mathrm{in}})}e^{\mp i m\varphi_{\mathrm{in}}}\right]. \tag{20}$$

III. BOUND STATES IN CONTINUUM

The BICs are source-free solutions of Eq. (16) which exist without the array being illuminated from the far zone. That yields a simple condition for BICs:

$$\det[\widehat{L}(k_0,k_z,\beta)] = 0. \tag{21}$$

In general, for given k_z, β the eigenfrequencies k_0 obtained from Eq. (21) through analytic continuation are complex. Thus, in search for BICs one has to trace the resonant eigenfrequencies to the point $\mathrm{Im}\{k_0\} = 0$. In this section we present the numerical results on BICs for arbitrary k_z, β in the range $a\beta < a\chi < 2\pi - a\beta$ for high-contrast dielectric rods, $\epsilon = 15$. The results are collected in Table I. The mode profiles of the BICs are shown in Fig. 2.

In regard to their position in momentum space the BICs can be split into four categories:

(i) In-Γ BICs with $k_z = 0$, $\beta = 0$. Such standing-wave BICs were first reported in Ref. [36]. In Table I, BICs 1–4 fall within this category. Notice the difference between BIC 1 and BIC 2 in Fig. 2. With the radiation channels being simply plane waves at $\beta = 0$, $k_z = 0$, it is evident that BIC 1 is the so-called symmetry protected bound state [36], whose mode shape is symmetrically mismatched with the mode shape of the radiation channels. Thus, BIC 1 is not "allowed" to radiate into the ambient medium. In contract, BIC 2 is not protected by symmetry. Numerical simulations show that finding the standing-wave BICs of the latter type is a complicated task since they only exist at a specific ratio R/a [36].

(ii) Off-Γ BICs with $k_z = 0$, $\beta \neq 0$. These states known as Bloch BICs [36] are localized waves traveling along the

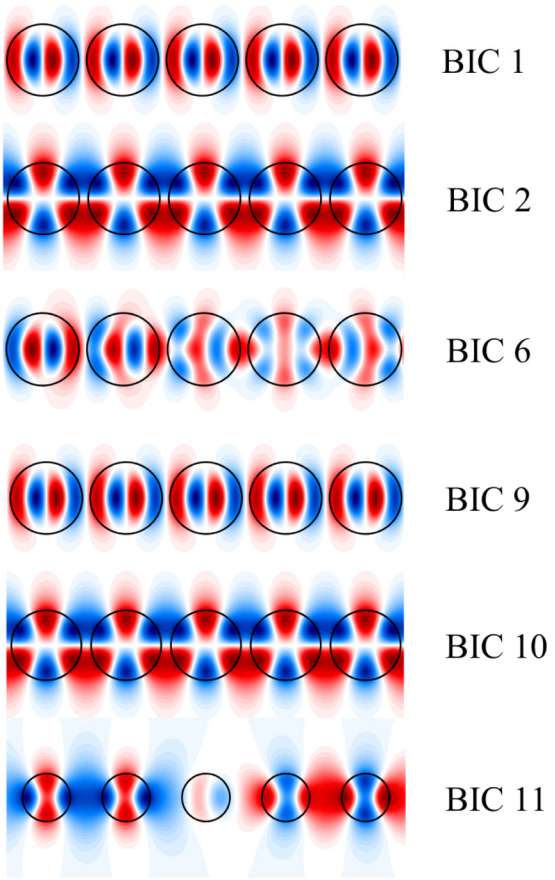

FIG. 2. Mode profiles of the BICs from Table I in the $x0y$ plane. The EM field is visualized as the real part of the z component of the electric field E_z.

array of rods in the x direction. By noticing that the system is symmetric with respect to the inversion of the x axis one can conclude that each Bloch BICs is twofold degenerate and, therefore, can be decomposed into two waves traveling in the opposite directions. The examples from Table I and Fig. 1 are BIC 5–8.

(iii) Off-Γ BICs with $k_z \neq 0$, $\beta = 0$. These BICs are traveling waves propagating along the axes of the rods. Again due to the symmetry these BICs are twofold degenerate. An examples of such BICs from Table I and Fig. 1 are BIC 9 and BIC 10. Notice the resemblance between BIC 1 and BIC 9 as well as between BIC 2 and BIC 10. This will be explained later on in the next section. It should be pointed out, although, that unlike BICs 1 and 2, which are TM standing waves, BICs 9 and 10 have nonzero component of magnetic field H_z (not shown here for brevity).

(iv) Off-Γ BICs with $k_z \neq 0$, $\beta \neq 0$. Such *bidirectional* BICs propagating both along the axes of the rods and the axis of the array to the best of our knowledge have never been reported in literature. These BICs are fourfold degenerate in a view of x,z-axis inversions. BIC 11 is the example of a bidirectional BIC from Table I and Fig. 1.

In summary to this section we point out that the values of parameters collected in Table I are not unique. Under small variations of R all the BICs, with exception of BIC 2, persist, merely changing their eigenfrequency and/or position in momentum space. Henceforth, we will use the same index for the BICs from each family generated by a continuous change of parameters.

IV. POLARIZATION SINGULARITIES AND TOPOLOGICAL CHARGE

The BICs are exceptional points in momentum space k_z, β. Once the wave vector is detuned from the exceptional point the BICs become leaky modes exponentially diverging in the far zone with $\mathrm{Im}\{k_0\} < 0$. Considering the evolution of BICs one has to secure that the BICs in question are supported by the same dispersion branch. A detailed numerical examination shows that BICs 2, 6, and 10 sit on the same dispersion branch, while BICs 1, 3, 4, 5, and 9 share a different dispersion branch of their own—hence the resemblance of the mode profiles shown in Fig. 1. The dependance of the imaginary part of the resonant eigenfrequency on β and k_z for the first zone supporting BICs is shown in Fig. 3(a) for $R/a = 0.43$. In Fig. 3(a) one can see three pronounced minima corresponding to the BICs.

The far-field profile of the leaky modes can be written as an expansion over the channel function (1) and (2):

$$\mathbf{E} = e\mathbf{E}_{TM} + h\mathbf{E}_{TE}, \tag{22}$$

where k_y in Eqs. (1) and (2) is now complex valued according to Eq. (5). Following Ref. [29] we project the far-field electric vector onto the $x0z$ plane. The electric field in the $x0z$ plane is a two-component vector

$$\bar{\mathbf{E}} = a_x\mathbf{x} + a_z\mathbf{z}. \tag{23}$$

By rotating the coordinates about the y axis,

$$z' = \cos(\vartheta)z - \sin(\vartheta)x, \tag{24}$$

$$x' = \sin(\vartheta)z + \cos(\vartheta)z, \tag{25}$$

one can transform the expansion coefficients a_x, a_z to the canonical form [40]

$$\frac{a_{z'}}{a_{x'}} = i\kappa, \tag{26}$$

where $0 \leqslant \kappa \leqslant 1$ is a real number, then the z' axis is aligned the main axis of the polarization ellipse. In Fig. 3(a) we plot κ across the leaky zone shown in Fig. 3(b). One can see that the far-field polarization is near linear in the domain of interest.

Since the polarization direction are uniquely specified by angle ϑ, we, in analogy with Ref. [29], can define the topological charge carried by the BIC as

$$q = \frac{1}{2\pi}\oint_C d\bar{\mathbf{k}} \cdot \nabla_{\bar{\mathbf{k}}}\vartheta(\bar{\mathbf{k}}), \tag{27}$$

where $\bar{\mathbf{k}} = [\beta, k_z]$, C is a closed simple path encircling the BIC in the counterclockwise direction in momentum space. Physically q defines how many times the polarization axis winds about the BIC along the loop C. The charge of the BICs is presented in Table I. Quite remarkably among the multiple charged BICs we found that BIC 2 is uncharged. In Fig. 3(c)–3(e) we show the polarization directions in the vicinity of BICs with $q = -1, 0, +1$. The global structure of the polarization directions of the leaky mode is shown in Fig. 3(f).

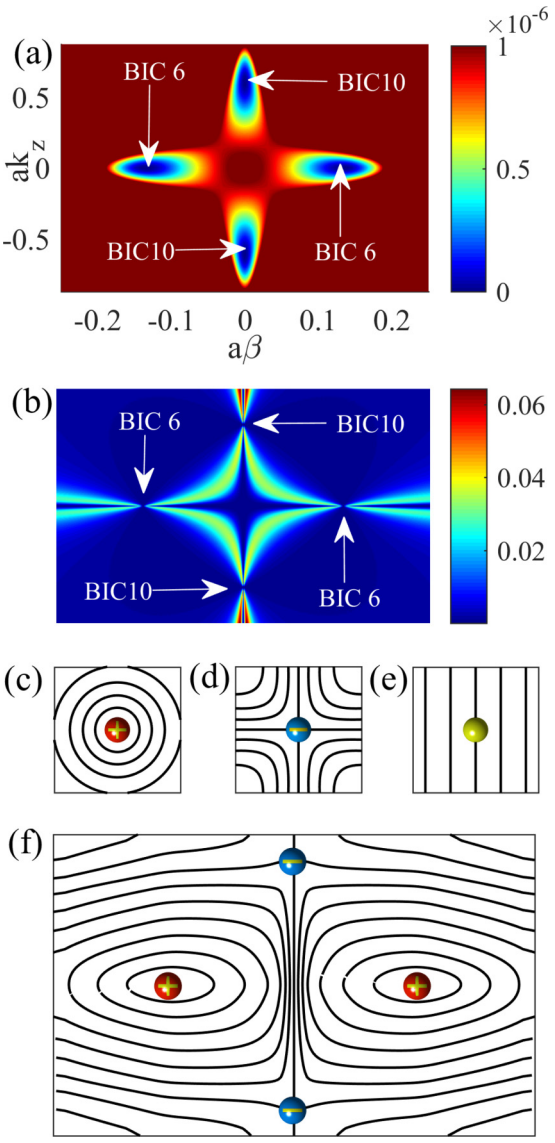

FIG. 3. (a) Dimensionless imaginary part of the eigenfrequency $a\mathrm{Im}\{k_0\}$ for the leaky zone supporting BIC 6 and BIC 10, $R/a = 0.43$. (b) Parameter κ in the same axes, $R/a = 0.43$. (c)–(e) Polarization direction in the vicinity of BICs 10, 6, and 2 from Table I, respectively. (f) Polarization directions in the same axis as in panel (a), $R/a = 0.43$.

In the points of singularity the far-field polarization direction is undefined. Hence, we can apply the arguments put forward in Ref. [29] and state that the corresponding resonant state cannot radiate because there is no way to assign a far-field polarization. In other words, the polarization singularity leads to a BIC. In the same manner the robustness of the BICs could be explained by conservation of the topological charge. One can also see now that BIC 2 is unstable since it carries no charge.

To guarantee the conservation of the topological charge it must be secured that the polarization direction is uniquely defined in all points except the BICs. The proposed definition of the topological charge becomes inconsistent only if the polarization ellipse evolves into a circle. It is a challenging

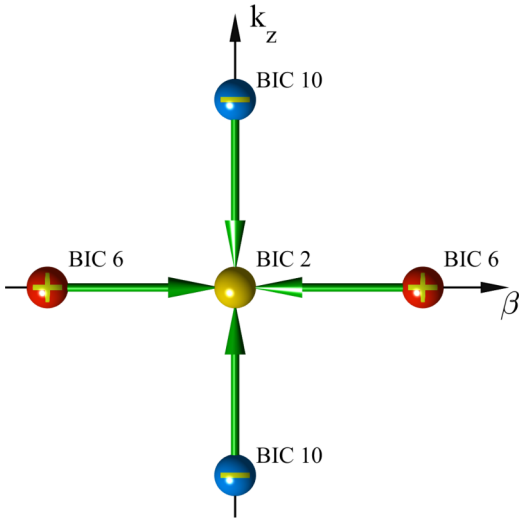

FIG. 4. Annihilation scenario for the dispersion branch shown in Fig. 3. Large green arrows show the direction BICs 6, 10 migrate in with increase of R.

mathematical task to prove that the far-field polarization is never circular for a given leaky zone. We, however, can argue that at least in the vicinity of the k_z,β axis the far-field polarization directions can be consistently defined for the whole Brillouin zone. Since the system possesses the mirror symmetry with respect to both the $x0y$ and $y0z$ planes, the leaky modes with $k_z \neq 0$, $\beta \neq 0$ are fourfold degenerate. On approaching any of the symmetry axes of the Brillouin zone (either $k_z = 0$, or $\beta = 0$), two degenerate leaky modes gradually merge one with the other. One the other hand, those modes are linked by the mirror operation which changes the handedness of the far-field polarization. It means that for $k_z = 0$, and $\beta = 0$ the polarization can only be linear and the far-field polarization pattern is always uniquely defined in the vicinity of the symmetry axes of the Brillouin zone.

V. EVOLUTION OF BOUND STATES IN THE CONTINUUM

In this section we numerically test the stability of the topologically charged BICs. The total topological charge prescribe to a certain leaky zone is a conserved quantity; therefore, as long as we stay in sector $N = 2$ in Fig. 1, the charged BICs cannot be destroyed under small variation of parameters, but rather migrate to another point in momentum space. The BICs can only emerge or disappear in pairs with the opposite topological charge [29,30]. In this section we describe the evolution of the BICs under variation of the radius of the rods R.

A. In-Γ annihilation

Let us first consider the lowest frequency dispersion branch that hosts BICs 2, 6, and 10 shown in Fig. 3. Starting from $R/a = 0.43$, we gradually increased the radius of the rods. It is found that both BICs 6 and 10 migrate towards the Γ point and eventually coalesce in BIC 2 which, as seen from Table I, carries no charge. With a further increase of R the BICs disappears from the system, i.e., four BICs have

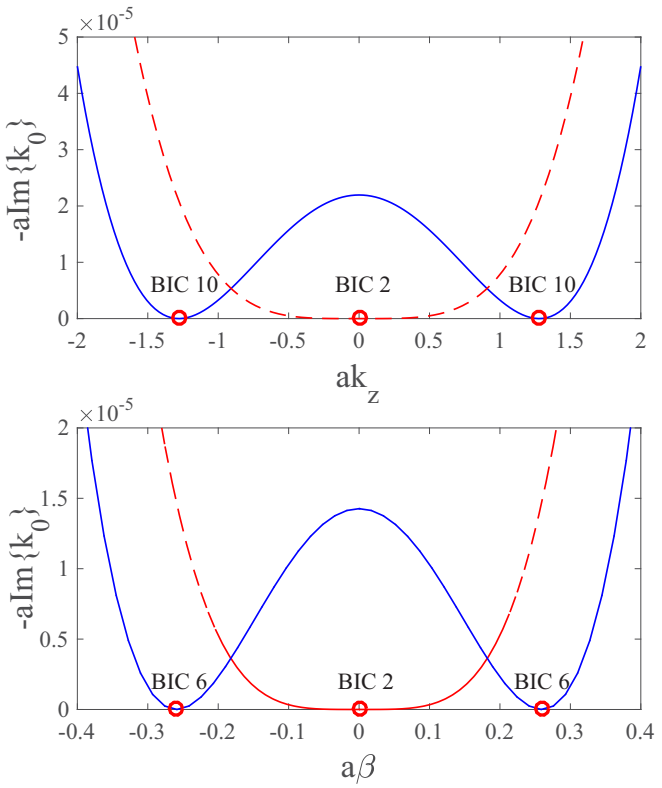

FIG. 5. Imaginary part of the eigenfrequency $-\mathrm{Im}\{k_0\}$ versus k_z (upper panel), $R = 0.4390a$ (solid blue line), $R = 0.44411a$ (dashed red line); and versus β (lower panel), $R = 0.44a$ (solid blue line), $R = 0.44411a$ (dashed red line).

been annihilated at the Γ point. In a view of the topological charge this picture is illustrated in Fig. 4. Let us consider the dependance of the imaginary part of the eigenfrequency $\mathrm{Im}\{k_0\}$ in more detail. As was demonstrated in Ref. [30], at the point of the total annihilation the dependance is approximated as

$$\mathrm{Im}\{k_0\} \sim (k - k_{\mathrm{BIC}})^2 (k + k_{\mathrm{BIC}})^2, \tag{28}$$

where k can be either k_z or β. As a consequence of this we obtain a *strong resonance* whose Q factor diverges as k^4 upon approaching the Γ point [41]. The dependance of the imaginary part of the resonant eigenfrequency at both annihilation and near-annihilation points is shown in Fig. 5. Again before annihilation one can clearly see two minima along the β and k_z axes. At the annihilation points the minima merge with the imaginary-part asymptotics given by Eq. (28).

B. In-Γ transformation

The second scenario is inherent to the higher-frequency dispersion branch with the total charge $q_{\mathrm{tot}} = +3$. Below the first critical value of the radius of the rods $R_1 = 0.440a$ we found three BICs with $q = +1$ and $\beta = 0$, two of them being propagating modes $k_z \neq 0$ BIC 9, and one standing wave $k_z = 0$ BIC 3. As before we examined the behavior of the BICs with increase of R. The simulations showed that when R achieves the first critical value R_1, the standing-wave BIC undergoes a transformation with two Bloch BIC 5 with $q = +1$ emerging at the Γ point, while the in-Γ standing-wave BIC changes the sign

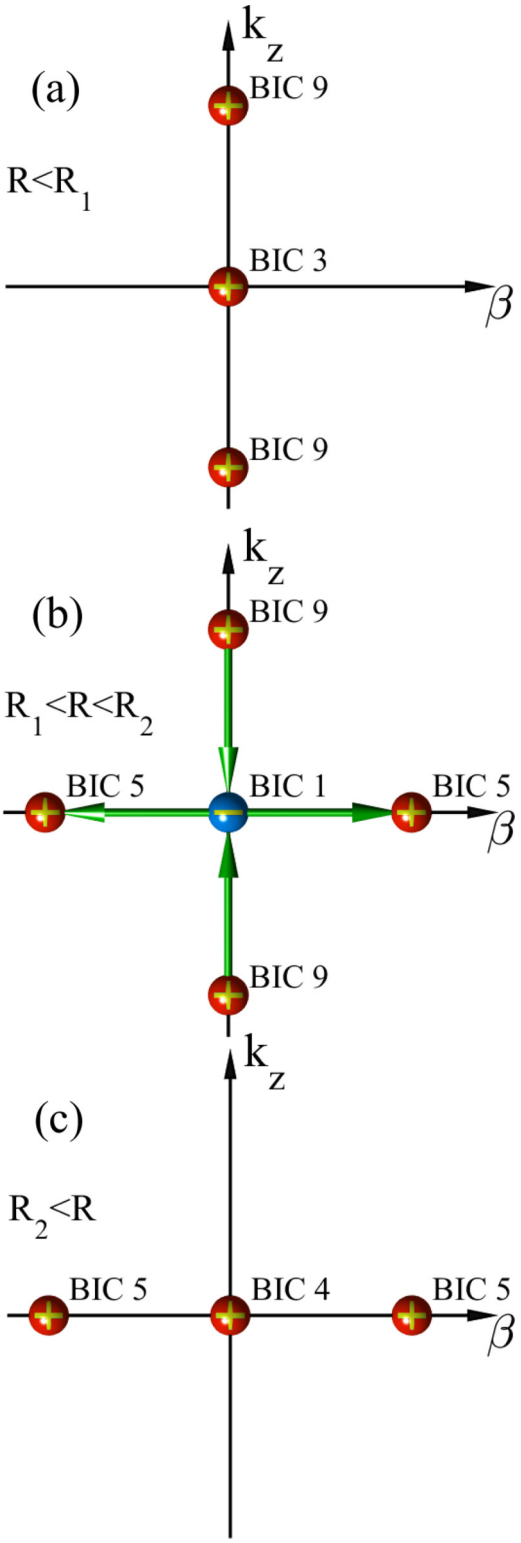

FIG. 6. In-Γ transformation of the topological charge for dispersion branch $q = 3$. (a) Three BICs at R below $R_1 = 0.440a$. (b) Bloch BICs emerge at $R = R_1$ and migrate away from the Γ point, while BICs migrate towards annihilation. (c) Three BICs with $q = 1$ after annihilation at the Γ point.

of the topological charge to $q = -1$ and becomes BIC 1. With a further increase of R two Bloch BIC 5 depart from the Γ point; meanwhile, BIC 9 approaches the Γ point along the k_z axis. At

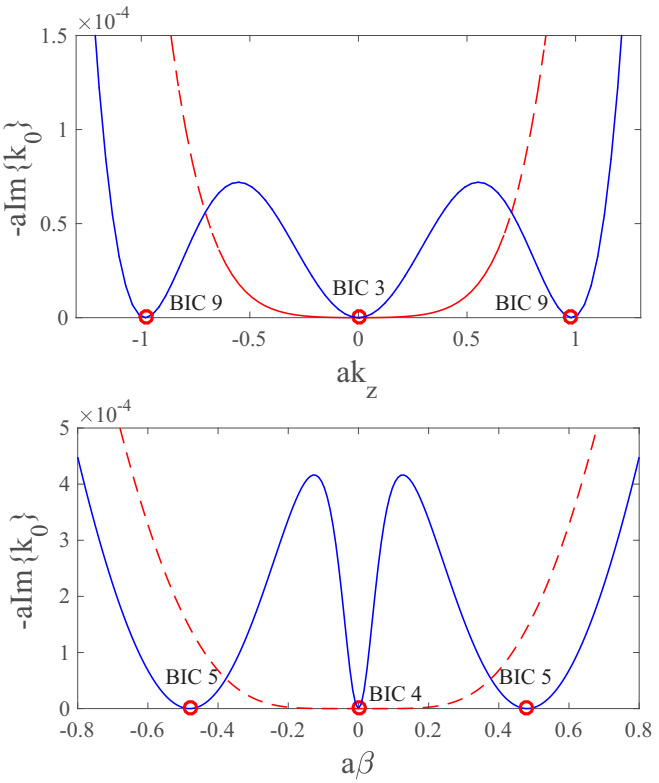

FIG. 7. Imaginary part of the eigenfrequency $-\mathrm{Im}\{k_0\}$ versus k_z (upper panel), $R = 0.4490a$ (solid blue line), $R = 0.4512a$ (dashed red line); and versus β (lower panel), $R = 0.4500a$ (solid blue line), $R = 0.4490a$ (dashed red line).

the second critical radius $R_2 = 0.4512a$ BIC 9 coalesces with the standing-wave BIC 1 with only one standing-wave BIC 4 surviving the annihilation. The topological charge is again preserved since for BIC 4 we have $q = +1$. We mention in passing that the second step in this scenario was previously described in Ref. [29]. The above scenario of the topological charge transformation is illustrated in Fig. 6.

The dependance of the imaginary part of the resonant eigenfrequency on k_z (upper panel) and β (lower panel) at both critical points is shown in Fig. 7. For $R < R_1$ we have three minima on the k_z axis which merge into a single minimum in the annihilation point. For $R > R_2$ the same picture is seen on the β axis.

C. Off-Γ annihilation

Finally, the third scenario describes the annihilation of the bidirectional BICs. From the topological viewpoint this scenario is identical to the in-Γ annihilation detailed in the previous section. Here, we restrict ourselves to presenting the generic picture in Fig. 8. Notice that the annihilation now occurs at the off-Γ point.

In summary, we have found that in all evolution scenarios the BICs sitting on the symmetry axes of the Brillouin zone are never destroyed, except through the total annihilation of the topological charge at the Γ point. This is consistent with the unique polarization picture in the vicinity of the symmetry axes described in the previous section. One may argue that in

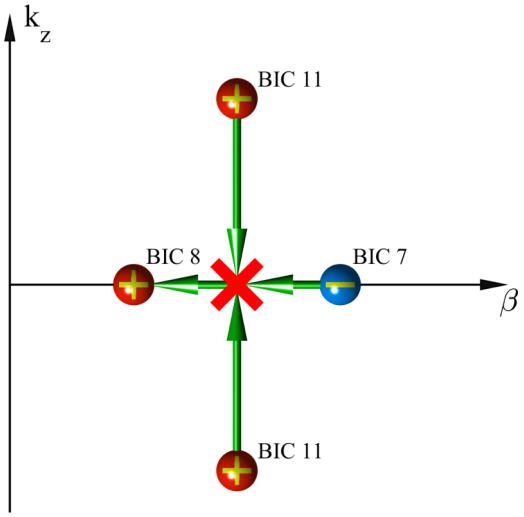

FIG. 8. Off-Γ annihilation of bidirectional BICs. The annihilation occurs at $R/a = 0.321$.

the course of evolution a BIC can depart from the symmetry axis to a sector of momentum space where the absence of circular polarization is not guaranteed. This, of course, can happen in the off-Γ creation or annihilation scenario. However, bidirectional BICs can only appear in pairs with the same topological charge because they are related by a point-group symmetry [29]. Thus, the third BIC of the opposite charge is always pinned to the symmetry axis. Therefore, we can conclude that all charged BICs sitting on the symmetry axes of the Brillouin zone are stable.

VI. FAR-FIELD SIGNATURES OF TOPOLOGICAL CHARGE

Let us now test whether the topological charge of the BICs can be detected in a physical experiment. To do that we computed transmission and reflection spectra of the array along the loop encircling topologically charged BIC 1 in momentum space k_z,β in the counterclockwise direction. In each step along the loop the incident wave remains circularly polarized. The wave vector of the incident wave as chosen according to the following formulas:

$$\beta = \delta \cos(\alpha), \tag{29}$$

$$k_z = \delta \sin(\alpha), \tag{30}$$

with $a\delta = 0.15$. In the vicinity of a BIC the scattering amplitudes are known to display a narrow Fano feature that collapses upon approaching the BIC [36,42]. A typical picture of the Fano resonance of the total transmittance $|e_t|^2 + |h_t|^2$ in the vicinity of BIC is shown in Fig. 9(a) for $\alpha = 0$. To stay definite in each step along the loop we tuned the frequency of the incident wave to the minimum of the Fano resonance. The evolution of the polarization ellipse of the transmitted radiation about BIC 1 is shown in Fig. 9(b) in the axes defined by the far-field scattering channels (2) and (1), One can see in Fig. 9(b) that the ellipse of polarization rotates about the singularity as prescribed by the topological charge.

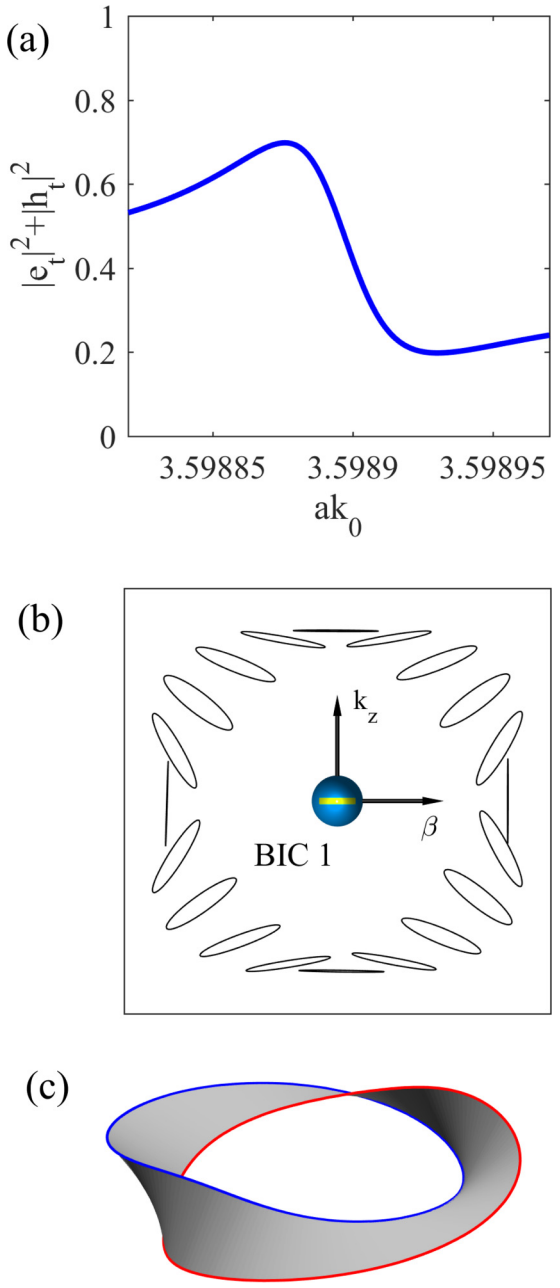

FIG. 9. Signature of topological charge in scattering by periodic arrays: (a) Fano feature in the total transmittance. (b) Polarization ellipses of the transmitted radiation in a loop about BIC 1. (c) Twist of polarization direction of the transmitted radiation in a loop about BIC 1.

That phenomenon could be qualitatively understood through a resonant excitation of the long-lived leaky mode associated with BIC 1. Once the leaky mode is excited, it suppresses the component of the background transmitted wave with the same polarization through destructive interference. Thus, the orientation of the suppressed component is aligned with the polarization direction of the leaky mode. We mention in passing that recently the resonant mode expansion has become a powerful computational tool for finding the reflection and transmission spectra of optical systems [43]. Presumably, the polarization picture could be explained in a view of the above reference. This, however, falls out of the scope of the present paper. Finally, to underscore the topological nature of the polarization singularity in Fig. 9(c) we present a three-dimensional ribbon plot of the polarization orientation along the loop C. One can clearly see a 2π twist, which cannot be removed unless C encircles a single topologically protected BIC.

VII. CONCLUSION

We have recovered the full picture of optical bound states in the radiation continuum (BICs) in high-contrast dielectric periodic arrays of dielectric rods. In particular, we found BICs propagating along the axes of the rods, and bidirectional BICs propagating along the axes of the rods and the axis of periodicity. It is shown that the BICs are exceptional points in the dispersion diagrams of leaky modes decaying into far-field radiation channels. In each point in momentum space those modes are characterized by the polarization ellipse of the far-field radiation. We demonstrated that, upon approaching a BIC in momentum space, the ellipses collapse so that the far-field radiation is nearly linearly polarized in the immediate vicinity of a BIC. This allowed us to apply the concept of polarization singularities developed in Ref. [29]. It is shown that the BICs carry a topological charge and, therefore, are robust against variations of parameters of the structure, given that the structure symmetry and periodicity are preserved. Thus, the concept of BICs as polarization singularities has been extended to the case of elliptic polarization. The behavior of BICs under variation of the radius of the rods has been studied numerically. It is found that evolution, creation, and annihilation of BICs obey the rule of charge conservation. Three scenarios of BICs annihilation are described. Finally, we demonstrated that the signature of the topological charge can be observed in the far field as the polarization singularities in the transmitted radiation, if the structure is illuminated by a circularly polarized plane wave. The finding presented here pave the way for engineering all-dielectric setups with beforehand desired polarization properties and high sensitivity to the orientation of the incident field.

ACKNOWLEDGMENTS

This work was supported by Ministry of Education and Science of Russian Federation (State Contract No. 3.1845.2017/4.6). We appreciate discussions with Almas F. Sadreev.

[1] C. W. Hsu, B. Zhen, A. D. Stone, J. D. Joannopoulos, and M. Soljačić, Nat. Rev. Mater. **1**, 16048 (2016).

[2] Y. Plotnik, O. Peleg, F. Dreisow, M. Heinrich, S. Nolte, A. Szameit, and M. Segev, Phys. Rev. Lett. **107**, 183901 (2011).

[3] S. Weimann, Y. Xu, R. Keil, A. E. Miroshnichenko, A. Tünnermann, S. Nolte, A. A. Sukhorukov, A. Szameit, and Y. S. Kivshar, Phys. Rev. Lett. **111**, 240403 (2013).

[4] C. W. Hsu, B. Zhen, J. Lee, S.-L. Chua, S. G. Johnson, J. D. Joannopoulos, and M. Soljačić, Nature (London) **499**, 188 (2013).

[5] T. Lepetit and B. Kanté, Phys. Rev. B **90**, 241103(R) (2014).

[6] R. A. Vicencio, C. Cantillano, L. Morales-Inostroza, B. Real, C. Mejía-Cortés, S. Weimann, A. Szameit, and M. I. Molina, Phys. Rev. Lett. **114**, 245503 (2015).

[7] Z. F. Sadrieva, I. S. Sinev, K. L. Koshelev, A. Samusev, I. V. Iorsh, O. Takayama, R. Malureanu, A. A. Bogdanov, and A. V. Lavrinenko, ACS Photonics **4**, 723 (2017).

[8] Y.-X. Xiao, G. Ma, Z.-Q. Zhang, and C. T. Chan, Phys. Rev. Lett. **118**, 166803 (2017).

[9] S. Venakides and S. P. Shipman, SIAM J. Appl. Math. **64**, 322 (2003).

[10] D. C. Marinica, A. G. Borisov, and S. V. Shabanov, Phys. Rev. Lett. **100**, 183902 (2008).

[11] E. N. Bulgakov and A. F. Sadreev, Phys. Rev. B **78**, 075105 (2008).

[12] Y. Yang, C. Peng, Y. Liang, Z. Li, and S. Noda, Phys. Rev. Lett. **113**, 037401 (2014).

[13] L. Ni, Z. Wang, C. Peng, and Z. Li, Phys. Rev. B **94**, 245148 (2016).

[14] L. Li and H. Yin, Sci. Rep. **6**, 26988 (2016).

[15] Y. Wang, J. Song, L. Dong, and M. Lu, J. Opt. Soc. Am. B **33**, 2472 (2016).

[16] X. Gao, C. W. Hsu, B. Zhen, X. Lin, J. D. Joannopoulos, M. Soljačić, and H. Chen, Sci. Rep. **6**, 31908 (2016).

[17] F. Monticone and A. Alù, New J. Phys. **19**, 093011 (2017).

[18] Z. Hu and Y. Y. Lu, J. Opt. Soc. Am. B **34**, 1878 (2017).

[19] L. Ni, J. Jin, C. Peng, and Z. Li, Opt. Express **25**, 5580 (2017).

[20] L. S. Li, J. Zhang, C. Wang, N. Zheng, and H. Yin, Phys. Rev. A **96**, 013801 (2017).

[21] V. Mocella and S. Romano, Phys. Rev. B **92**, 155117 (2015).

[22] J. W. Yoon, S. H. Song, and R. Magnusson, Sci. Rep. **5**, 18301 (2015).

[23] E. N. Bulgakov and D. N. Maksimov, Opt. Express **25**, 14134 (2017).

[24] A. Taghizadeh and I.-S. Chung, Appl. Phys. Lett. **111**, 031114 (2017).

[25] A. Kodigala, T. Lepetit, Q. Gu, B. Bahari, Y. Fainman, and B. Kanté, Nature (London) **541**, 196 (2017).

[26] B. Bahari, F. Vallini, T. Lepetit, R. Tellez-Limon, J. H. Park, A. Kodigala, Y. Fainman, and B. Kante, Integrated and steerable vortex lasers using bound states in continuum, arXiv:1707.00181.

[27] J. M. Foley, S. M. Young, and J. D. Phillips, Phys. Rev. B **89**, 165111 (2014).

[28] X. Cui, H. Tian, Y. Du, G. Shi, and Z. Zhou, Sci. Rep. **6**, 36066 (2016).

[29] B. Zhen, C. W. Hsu, L. Lu, A. D. Stone, and M. Soljačić, Phys. Rev. Lett. **113**, 257401 (2014).

[30] E. N. Bulgakov and D. N. Maksimov, Phys. Rev. Lett. **118**, 267401 (2017).

[31] L. Yuan and Y. Y. Lu, Opt. Lett. **42**, 4490 (2017).

[32] N. D. Mermin, Rev. Mod. Phys. **51**, 591 (1979).

[33] S. Henshaw and A. F. Izmaylov, Topological origins of bound states in the continuum for systems with conical intersections, arXiv:1710.08981.

[34] Y. Zhang, A. Chen, W. Liu, C. W. Hsu, F. Guan, X. Liu, L. Shi, L. Lu, and J. Zi, Observation of optical vortices in momentum space, arXiv:1709.03648.

[35] Y. Guo, M. Xiao, and S. Fan, Phys. Rev. Lett. **119**, 167401 (2017).

[36] E. N. Bulgakov and A. F. Sadreev, Phys. Rev. A **90**, 053801 (2014).

[37] L. Yuan and Y. Y. Lu, J. Phys. B: At., Mol. Opt. Phys. **50**, 05LT01 (2017).

[38] K. Yasumoto, in *Electromagnetic Theory and Applications for Photonic Crystals*, edited by K. Yasumoto (CRC Press, New-York, 2005).

[39] I. Y. Polishchuk, A. A. Anastasiev, E. A. Tsyvkunova, M. I. Gozman, S. V. Solov'ov, and Y. I. Polishchuk, Phys. Rev. A **95**, 053847 (2017).

[40] G. J. Gbur, in *Singular Optics*, edited by E. R. Pike and R. G. W. Brown (CRC Press, 2017).

[41] L. Yuan and Y. Y. Lu, Phys. Rev. A **95**, 023834 (2017).

[42] C. Blanchard, J.-P. Hugonin, and C. Sauvan, Phys. Rev. B **94**, 155303 (2016).

[43] M. B. Doost, W. Langbein, and E. A. Muljarov, Phys. Rev. A **90**, 013834 (2014).